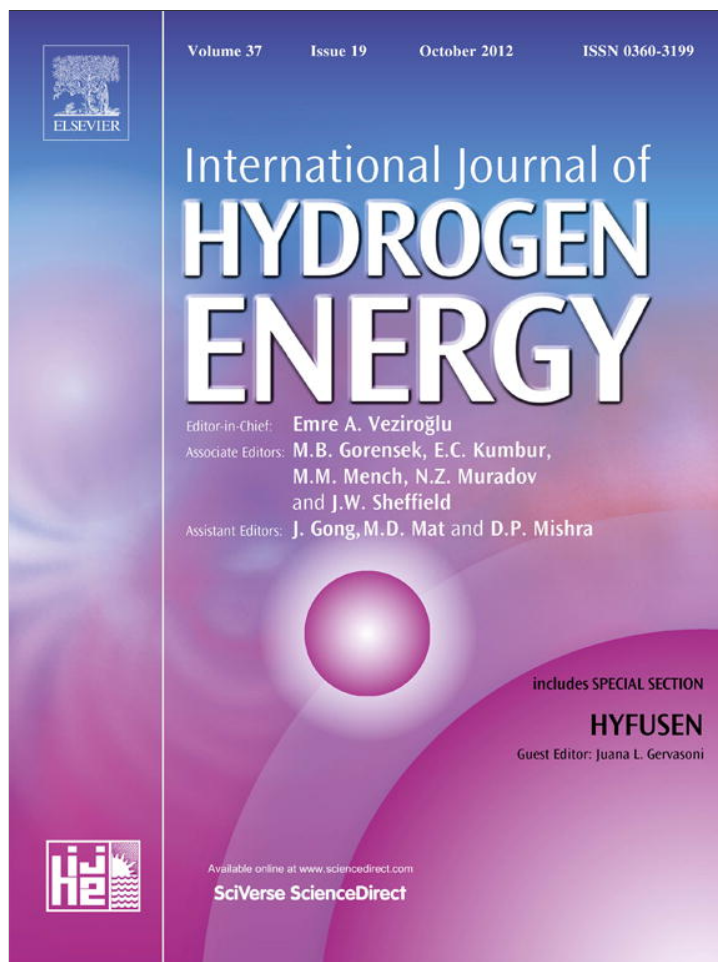


Provided for non-commercial research and education use.
Not for reproduction, distribution or commercial use.



This article appeared in a journal published by Elsevier. The attached copy is furnished to the author for internal non-commercial research and education use, including for instruction at the authors institution and sharing with colleagues.

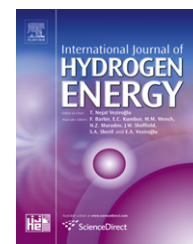
Other uses, including reproduction and distribution, or selling or licensing copies, or posting to personal, institutional or third party websites are prohibited.

In most cases authors are permitted to post their version of the article (e.g. in Word or Tex form) to their personal website or institutional repository. Authors requiring further information regarding Elsevier's archiving and manuscript policies are encouraged to visit:

<http://www.elsevier.com/copyright>

Available online at www.sciencedirect.com

SciVerse ScienceDirect

journal homepage: www.elsevier.com/locate/ije

A model for atomic hydrogen–bimetal interactions

S. Simonetti^{a,b,*}, C. Canto^{c,2}

^a Universidad Tecnológica Nacional, 11 de Abril 461, 8000 Bahía Blanca, Argentina

^b Universidad Nacional del Sur, Av. Alem 1253, 8000 Bahía Blanca, Argentina

^c Universidad Autónoma de Campeche, Av. Agustín Melgar s/n Col. Buenavista, 24039 San Francisco de Campeche, Mexico

ARTICLE INFO

Article history:

Received 8 October 2011

Accepted 12 December 2011

Available online 31 December 2011

Keywords:

Alloy

Iron

Nickel

Hydrogen

Modelling studies

ABSTRACT

The adsorption of atomic H on the bimetallic FeNi(111) surface has been studied by ASED-MO tight binding calculations. The energy of the system was calculated by the atom superposition and electron delocalization molecular orbital (ASED-MO) method. Seven H locations on the alloy surface were selected and the hydrogen atom was positioned in their energy minima configurations.

By ASED-MO calculations, the H atom presents its most stable position when it bonds on top Fe atom at 1.5 Å and, on bridge Fe–Fe at 0.7 Å, respectively. In these cases, the strength of the local Fe–Fe bond decreases 12% and 33% of its original bulk value, respectively. As a consequence of Fe–H interaction, a decohesion mechanism in the Fe–Fe bond could be evidenced. On the other hand, the Fe–Ni and Ni–Ni superficial bonds are slightly modified between 0.4 and 2%. A discussion based on electronic structure studies using the concept of density of states (DOS) and crystal orbital overlap population (COOP) curves is presented.

Copyright © 2011, Hydrogen Energy Publications, LLC. Published by Elsevier Ltd. All rights reserved.

1. Introduction

While the world's oil reserves are being rapidly depleted, the supply of hydrogen remains virtually unlimited and produces no air pollutants. Hydrogen can be produced from several sources, reducing our dependence on petroleum.

Hydrogen can be obtained from renewable sources (i.e. bio-ethanol) through thermal or catalytic processes. A high yield of hydrogen can be achieved using noble metal based catalysts in auto-thermal reforming of ethanol (ATRE), while a low hydrogen yield is obtained using non-precious metal catalysts due to their limited catalytic activity and stability [1–3].

Iron promoted nickel based catalyst has been developed for high yield hydrogen generation through ethanol reforming [4].

The reaction results show a remarkable improved durability in catalytic activity as well as selectivity to hydrogen in auto-thermal reforming (ATR) is obtained: Over the 10 wt.% iron-loading nickel catalyst, conversion of ethanol at 99.61% and selectivity of hydrogen around 115% are kept at 600 °C during a 30-h test, while that of iron-free sample decreases sharply from 85.10% to 19.71% on hydrogen selectivity within a 26-h test. The improved durability is attributed to the synergistic effect of the NiAl₂O₄–FeAl₂O₄ mixed crystals that are more resistant to sintering and oxidation in the oxidative atmosphere of ATR.

The decomposition of a C₂H₄/CO/H₂ reactant mixture over a series of Fe–Ni catalysts has been investigated by Park and Baker. The co-adsorption of the two carbon-containing gases

* Corresponding author. Universidad Tecnológica Nacional, 11 de Abril 461, 8000 Bahía Blanca, Argentina. Tel.: +54 291 4555220.

E-mail address: ssimonet@uns.edu.ar (S. Simonetti).

¹ Tel.: +54 291 4595141; fax: +54 291 4595142.

² Tel.: +981 8119800x62800.

0360-3199/\$ – see front matter Copyright © 2011, Hydrogen Energy Publications, LLC. Published by Elsevier Ltd. All rights reserved.

doi:10.1016/j.ijhydene.2011.12.087

produces major modifications in the behaviour of the bimetallic surfaces, resulting in a substantial increase in the decomposition of the olefin over all the bimetallic powders with this effect being most pronounced on the iron-rich systems. The perturbations in the electronic properties of the bimetallic surfaces are considered to be a contributory factor to the change in the catalytic action. A reversible deactivation/reactivation phenomenon was shown to exist for iron-rich bimetallic catalysts. It was interesting to find that under the same conditions this behaviour did not prevail with nickel-rich bimetallic catalysts, which merely exhibited the traditional irreversible deactivation [5].

Investigations have reported that binary Fe–M catalysts (M = Ni, Mo, or Pd) supported on high surface area γ -alumina decreased the decomposition temperatures of methane, ethane, and propane by 400–500 °C and yielded 70–90% hydrogen in the temperature range of 650–800 °C [6,7].

Hirao et al. have investigated the reaction between iron–nickel alloys, Fe₉₀Ni₁₀ and Fe₉₅Ni₅, and water at high pressures and high temperatures. The reaction of iron–nickel alloys with water depends on pressure. The authors found that the amount of hydride formed by the reaction is smaller in the iron–nickel–water system than in the iron–water system, although the hydrogen content in iron–nickel hydride is not significantly different from that in iron hydride. The results indicate that the existence of nickel in iron tends to reduce the amount of hydrogen supplied [8].

The dependence of the rate of the production of biogas upon the concentration of nickel and iron at sub-toxic concentration and monitored its composition as amount of hydrogen, methane and carbon dioxide have been investigated by Aresta et al. The results of the investigations show that the addition of any of the listed metals to the sludge may cause the production of a higher amount of biogas and influence the methane or carbon dioxide percentage. Conversely, the effect on the hydrogen production depends upon the metal added, the age of the active sludge used, and its adaptation to the substrate. As a general feature, during the acidogenesis phase, nickel reduces, while iron increases, the percentage of dihydrogen in the biogas [9].

NiFe alloys coatings were electrochemically deposited on copper net supports. The results are discussed in detail with emphasis on routes to increase the iron content and the surface roughness. The NiFe-3 alloy (with a molar concentration of Ni²⁺:Fe²⁺ of 4:6 in plating bath) was found to be the best suitable cathode material. The iron content of the obtained alloys increases with the content of iron in electrolyte [10].

Energy of metal–metal (Me–Me) and metal–hydrogen (Me–H) bonds in hydrogen-free and hydrogen-charged fcc iron, nickel, and iron–nickel alloys are ab initio calculated. It is shown that short-range decomposition of Fe–Ni solid solution and difference in Fe–H and Ni–H bonds are responsible for splitting of γ reflections in the X-ray diffraction patterns, which is at variance with the common interpretation in terms of a hydrogen-caused γ^* phase. X-ray diffraction measurements confirm the absence of miscibility gap in the FeNi–H solid solution and its occurrence in Ni–H. Results of calculations are consistent with the absence of H–H pairs in pure nickel [11].

In this paper we studied by ASED-MO tight binding calculations, the H chemisorption on the FeNi(111) alloy surface. We also analyzed the electronic structure and bonding during the adsorption phenomena. The theory and model are described in the next section.

2. Theoretical method and adsorption model

Our calculations were performed using the ASED-MO method an approximate molecular orbital tight binding scheme [12]. This method captures well the essential orbital interactions in chemisorption. The interaction between the H atom and the FeNi(111) surface was studied using a two dimensional slab of finite thickness, so as to better simulate the semi-infinite nature of the metallic surface. A three-layer slab was employed as a compromise between computational economy and reasonable accuracy. The FeNi(111) surface was represented by 108 atoms (50:50) distributed in three layers (FCC arrangement) of 36 atoms (see Fig. 1(a)).

The adsorption energy E_{ads} values were calculated from the energy difference:

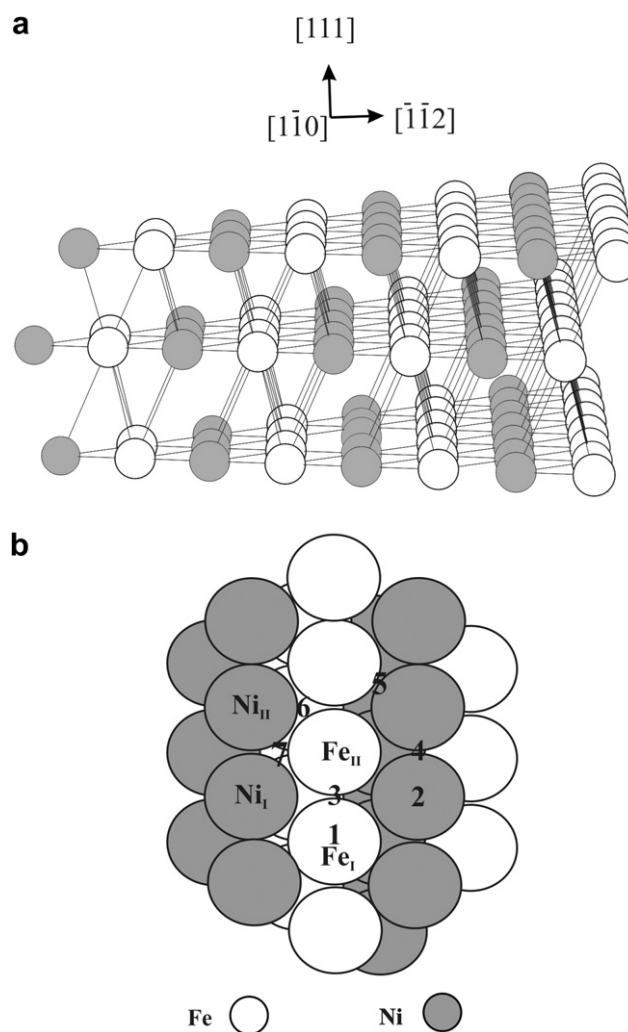


Fig. 1 – (a) The FeNi(111) slab. (b) Schematic top view of the H adsorption sites on the FeNi(111) surface.

$$E_{\text{ads}} = E_{\text{T}}(\text{FeNi}/\text{H}) - E_{\text{T}}(\text{FeNi}) - E_{\text{T}}(\text{H}) \quad (1)$$

where FeNi/H, H and FeNi refer to H atom-on-slab system, the free H atom and the bare iron–nickel surface, respectively.

The density of states (DOS) and the crystal orbital overlap population (COOP) curves for the FeNi–H system were calculated in order to analyze the atom–surface interactions using the YAeHMOP code [13]. The COOP curve is an energy-resolved plot of the overlap population-weighted density of states. Integration of the COOP curve up to the Fermi level gives the total overlap population (OP).

3. Results and discussions

Seven H locations on the alloy surface were selected and the hydrogen atom was positioned in their energy minima configurations. The adsorption sites for the H on the FeNi(111) surface are shown in Fig. 1 (b). Table 1 presents the adsorption minimum energy and the corresponding surface–H distance for each sites. For such adsorption sites, the total energy difference is negative, then, the adsorption is favourable in all sites. We can see that sites 1 and 3 are the most stables and corresponding to H located, on Fe top site and on the Fe–Fe bridge site, respectively. The energy difference between sites 1 and 3 is 0.11 eV while the equilibrium distances from H to the surface are 1.50 Å and 0.70 Å, respectively.

Regarding the electronic structure, we calculated the density of states (DOS) and the crystal orbital overlap population (COOP) curves for the FeNi/H system in order to analyze the adsorbate–surface interactions. Fig. 2(a) shows the DOS plots for the FeNi(111)/H system. The alloy d states form a band starting at –14 eV with a bandwidth of 7 eV. If we compare with the total DOS of the isolated FeNi(111) surface (Fig. 2(b)), the more noticeable difference is the small peak that appear at about –15.5 eV that corresponds to the H state after adsorption. The small contribution of the H to DOS is due to its low concentration. A major view is shown in Fig. 2(c) that presents a plot of the H state projection. The Fermi energy of the metal surface moves slightly, because of the finite thickness of the slab and electron transfer between slab and adsorbate.

Tables 2 and 3 present the atomic orbital occupation and the OP values for the atoms that participate in the FeNi–H interaction. For the H adsorption on site 1, the hydrogen atom bond on top Fe_I with an OP of 0.645. The COOP curves for the

Table 1 – Minimum energy position and the corresponding hydrogen–surface distances for the H adsorption sites on the FeNi(111) surface.

H adsorption site	C–surface distance (Å)	Energy (eV)
1	1.5	–5.87
2	1.5	–5.45
3	0.7	–5.76
4	1.2	–5.31
5	1.1	–5.50
6	0.9	–5.60
7	0.9	–5.38

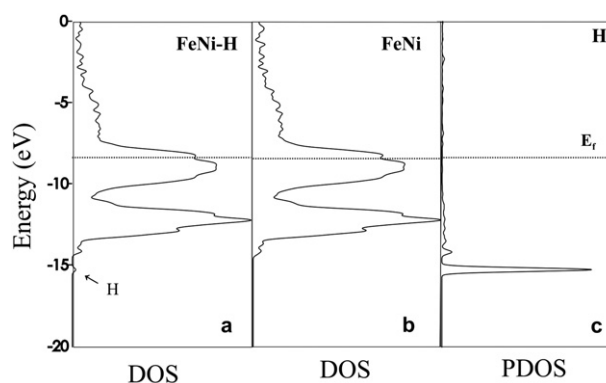


Fig. 2 – (a) Total DOS for the FeNi(111)/H system, (b) total DOS for the clean FeNi(111) surface and (c) projected DOS for H on the FeNi(111) surface.

Fe_I–H interaction are shown in Fig. 3(a), as we can see it corresponds to a bonding interaction. The Fe–H interaction mainly involves p_z and s orbitals of Fe_I whose populations increase 82% and decrease 16%, respectively, comparing with the clean surface (see Table 2). The d_{z^2} and p_y populations of Fe_I decrease to about 9% and 6%, respectively; while the rest of the Fe_I orbital populations is modified less than 2%. The Fe_I–Fe_{II} OP decrease to about 12% after the H adsorption; the Fe_{II} major changes are noticed in p_y (40%), d_{yz} (8%) and p_z (6%) atomic orbitals whose populations decrease comparing with the clean surface. We can conclude that the changes are due to the Fe_I–H interaction that is mainly formed at expense of the Fe_I–Fe_{II} neighbouring bond (see Table 3). There is observed an electron transfer from Fe and Ni nearest neighbours to the H atom. The Fe–Ni and Ni–Ni nearest neighbouring bonds are slightly modified after H location, the Fe–Ni bond strength is fortified to about 1% and the Ni–Ni bond strength decrease to about 0.4% after the H adsorption. The major changes are observed in s , p_x and p_z Ni orbital whose populations decrease less than 3%. No evidence of Ni–H interaction is observed. The presence of nickel in the alloy composition could reduce the H

Table 2 – Atomic orbital occupations for the H atom and their neighbouring atoms.

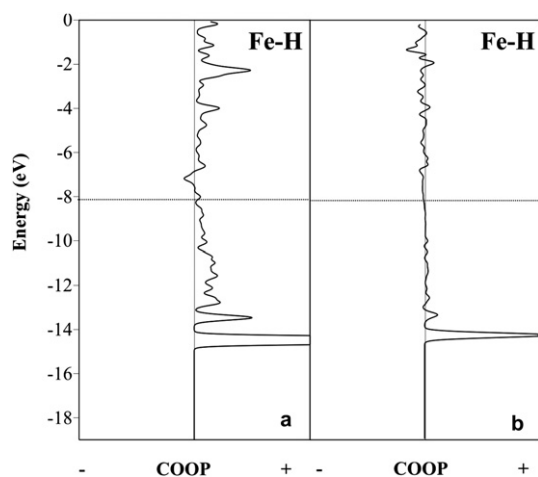
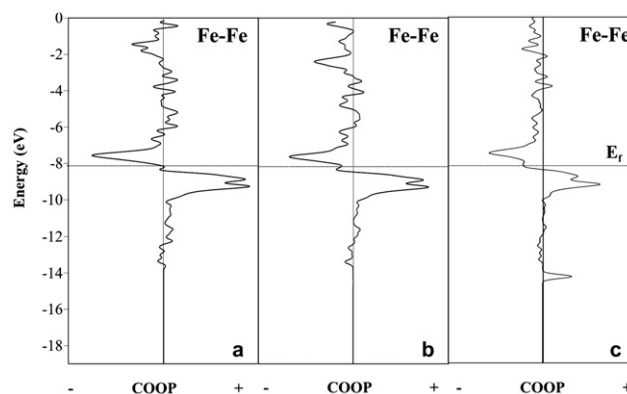
	s	p_x	p_y	p_z	$d_{x^2-y^2}$	d_{z^2}	d_{xy}	d_{xz}	d_{yz}
<i>H on top Fe</i>									
Fe _I	0.501	0.080	0.031	0.232	1.158	1.037	0.990	1.288	1.150
Fe _{II}	0.583	0.082	0.019	0.037	1.134	1.106	0.994	1.310	1.062
Ni _I	0.846	0.309	0.306	0.295	1.890	1.866	1.863	1.911	1.909
H	1.459								
<i>H on bridge Fe–Fe</i>									
Fe _I	0.520	0.080	0.023	0.105	1.141	1.122	0.995	1.277	0.945
Fe _{II}	0.522	0.082	0.023	0.105	1.115	1.121	0.995	1.307	0.969
Ni _I	0.839	0.311	0.307	0.299	1.888	1.866	1.863	1.917	1.910
H	1.521								
<i>Isolated Fe–Ni surface</i>									
Fe _I	0.594	0.081	0.033	0.042	1.134	1.133	0.994	1.313	1.157
Fe _{II}	0.594	0.080	0.031	0.039	1.173	1.091	0.990	1.286	1.155
Ni _I	0.833	0.312	0.308	0.301	1.891	1.863	1.863	1.917	1.910

Table 3 – Metal–H interactions and major changes in the metallic OP values.

Bond	OP
<i>H on top Fe</i>	
Fe _I –Fe _{II}	0.229
Fe _I –Ni _I	0.178
Ni _I –Ni _{II}	0.265
Fe _I –H	0.645
<i>H on bridge Fe–Fe</i>	
Fe _I –Fe _{II}	0.175
Fe _I –Ni _I	0.178
Fe _{II} –Ni _I	0.177
Ni _I –Ni _{II}	0.264
Fe _I –H	0.244
Fe _{II} –H	0.243
<i>Isolated Fe–Ni surface</i>	
Fe _I –Fe _{II}	0.262
Fe _I –Ni _I	0.176
Fe _{II} –Ni _I	0.174
Ni _I –Ni _{II}	0.266

accumulation. Nickel can prevent H deposition by reducing catalytic activity for the reaction of H on the surface [8,9]. A study reveals that Ni and Fe may act as either competing or cooperative catalyst components in Ni–Fe based steel alloy. During partial oxidation of methane it is resulted in suppression of Ni catalytic activity in favour of Fe. Interaction between Ni and Fe during non-oxidative conversion leads to cooperative effect; the activity of bimetallic catalyst increases as compared with monometallic one [14].

For the H adsorption on site 2, the H atom locates on Fe_I–Fe_{II} bridge site, the Fe–H interactions are formed and both Fe_I–H and Fe_{II}–H OPs are similar and smaller than the Fe_I–H OP when the H is located on top Fe_I. A comparison of the Fe–H OPs can be seen in Fig. 3(a) and (b). After adsorption, the most affected are the p_z , p_y , d_{yz} and s orbitals of both Fe_I and Fe_{II} whose populations modified between 60–63%, 25–31%, 16–18% and 12–13%, respectively. The population of the rest of both Fe_I and Fe_{II} orbitals is modified less than 5% (see Table

**Fig. 3 – COOP curves for the Fe–H interaction, when the H atom is (a) on top Fe and (b) on bridge Fe–Fe.****Fig. 4 – COOP curves for the Fe–Fe interaction, (a) before H adsorption, (b) after H adsorption (H on top Fe atom) and (c) after H adsorption (H on bridge Fe–Fe).**

2). The Fe_I–Fe_{II} OP decrease to about 33% due the Fe_I–H and Fe_{II}–H interactions formed on the FeNi(111) surface (see Table 3). There is observed an electron transfer from Fe nearest neighbours to Ni and H atoms. The neighbouring Fe_I–Ni_I and Fe_{II}–Ni_I bonds strength increase less than 2% and the Ni_I–Ni_{II} bond strength decrease to about 0.8%. As a consequence of the formed Fe–H interactions, we observed a small Ni–Ni bond weakening while Ni atoms increase its bonding with neighbouring Fe atoms after the H adsorption. Ni–H interaction is not observed.

A detrimental effect on the Fe–Fe bonds is observed after the H adsorption on the FeNi(111) surface. We have reported a Fe–Fe bond weakening between 12 and 33% for the studied two major adsorption sites. Fig. 4 shows a comparison plot of the Fe–Fe superficial bond, before and after the H adsorption. The integration of the Fe–Fe COOP curves up to the Fermi level gives smaller total overlap populations for the H chemisorption's systems (Fig. 4(b) and (c)) compared with the clean surface (Fig. 4(a)) confirming the Fe–Fe bond weakening after adsorption.

4. Conclusions

We have analyzed at theoretical level, the adsorption of H on FeNi(111) by tight binding calculations. Different sites on the surface were selected in order to establish the preferential H adsorption location and the optimum H–surface distance. The two most stable sites for H on FeNi(111) are those where H bonds on top Fe at 1.50 Å to the surface and the H bonds on the Fe–Fe bridge site at 0.70 Å above the surface.

We found that the minimum energy site corresponds to the H bonding on top Fe. Fe–H bond is formed on the FeNi surface and the interaction is mainly due to the overlaps between the H s orbital with the p_z , s , d_{z^2} and p_y Fe orbitals. As a consequence, it is observed a Fe–Fe bond weakening of 12%. On the other hand, when the H is located on the Fe–Fe bridge site, the Fe–H interactions weaken the Fe–Fe nearest bonds to about 33% with mainly participation of p_z , p_y , s and d_{yz} Fe orbitals. In general, after H adsorption, the Fe–Ni and Ni–Ni bonds are slightly affected. The Ni–H interaction is not evidence on the FeNi(111) surface.

Acknowledgements

Our work was supported by the MINCyT–CONACyT Scientific-Technological Cooperation Program (MX/09/11), PIP 0103 (CONICET), PGI 25/B029 (UTN), PGI 24/ZFO3 (UNS). Simonetti is member of CONICET-Argentina.

REFERENCES

- [1] Milliken JA, Joseck F, Wang M, Yuzugullu E. The advanced energy initiative. *J Power Sources* 2007;172:121–31.
- [2] Momirlan M, Veziroglu T. Recent directions of world hydrogen production. *Renew Sustain Energy Rev* 1999;3:219–31.
- [3] Vaidya PD, Rodrigues AE. Insight into steam reforming of ethanol to produce hydrogen for fuel cells. *Chem Eng J* 2006; 117:39–49.
- [4] Huang L, Xie J, Chen R, Chu D, Hsu A. Improved durability of iron promoted non-precious metal catalysts for hydrogen generation through bio-ethanol reforming. *Meet Abstr Electrochem Soc* 2008;802:828.
- [5] Park C, Baker TK. Carbon deposition on iron–nickel during interaction with ethylene–carbon monoxide–hydrogen mixtures. *J Catal* 2000;190:104–17.
- [6] Shah N, Wang Y, Panjala D, Huffman GP. Pure hydrogen production by partial dehydrogenation of cyclohexane and methyl cyclohexane over nanotube supported Pt and Pd catalysts. *Energy Fuels* 2004;18:727–35.
- [7] Wang Y, Shah N, Huffman GP. Simultaneous production of hydrogen and carbon nanostructures by decomposition of propane and cyclohexane over alumina supported binary catalysts. *Catal Today* 2005;99:359–64.
- [8] Hirao N, Ohtani E, Kondo T, Kikegawa T. Iron–nickel–water system under high pressure and high temperature. *American Geophysical Union*; 2004. Fall Meeting, abstract #T41B-1182.
- [9] Arestaab M, Narraccib M, Tommasi I. Influence of iron, nickel and cobalt on biogas production during the anaerobic fermentation of fresh residual biomass. *Chem Ecol* 2003;19: 451–9.
- [10] Poroch-Seritan M, Gutt S, Gutt G, Bobu MM. Synthesis and characterization of nickel iron alloys by electrodeposition. *Traian Severin*, 18–20. 5. 2010, Roznov pod Radhostem, Czech Republic, EU, Metal 2010, Charleston South Carolina, United States.
- [11] Movchan DN, Shyvanyuk VN, Shanina BD, Gavriljuk VG. Atomic interactions and hydrogen-induced γ^* phase in fcc iron–nickel alloy. *Phys Status Solidi (a)* 2010;207: 1796–801.
- [12] Anderson A, Nath K. Atom-superposition and electron-delocalization tight-binding band theory. *Phys Rev B* 1990;41: 5652–60.
- [13] Landrum G, Glassey W. Yet another extended Hückel molecular orbital package (YAEHMOP). Ithaca, NY: Cornell University; 2004.
- [14] Mordkovich VZ, Dolgova EA, Karaeva AR, Kharitonov DN, Maslov IA, Kamenev AA, et al. Synthesis of carbon nanotubes by catalytic conversion of methane: competition between active components of catalyst. *Carbon* 2007;45:62–9.